ACS APPLIED MATERIALS & INTERFACES

Letter

www.acsami.org

Ultrahigh Thermal Rectification in Pillared Graphene Structure with Carbon Nanotube−Graphene Intramolecular Junctions

Xueming Yang,*[,†,‡] Dapeng Yu,[‡] Bingyang Cao,*[,†] and Albert C. To[§]

[†]Key Laboratory for Thermal Science and Power Engineering of Ministry of Education, Department of Engineering Mechanics, Tsinghua University, Beijing 100084, China

[‡]Department of Power Engineering, North China Electric Power University, Baoding 071003, China

[§]Department of Mechanical Engineering and Materials Science, University of Pittsburgh, Pittsburgh, Pennsylvania 15260, United States

Supporting Information

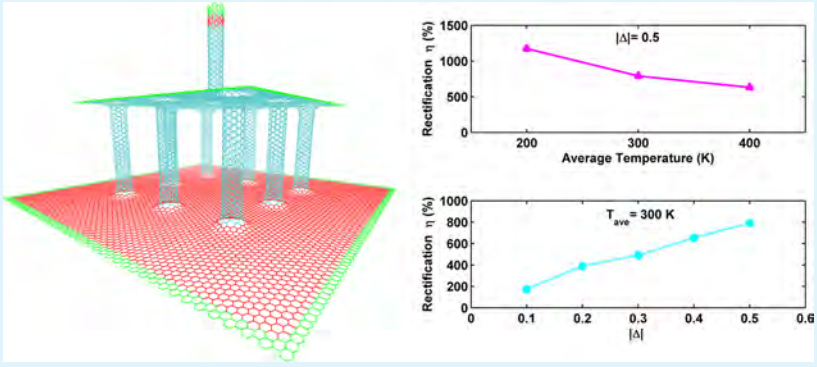

ABSTRACT: In this letter, graded pillared graphene structures with carbon nanotube−graphene intramolecular junctions are demonstrated to exhibit ultrahigh thermal rectification. The designed graded two-stage pillared graphene structures are shown to have rectification values of 790.8 and 1173.0% at average temperatures 300 and 200 K, respectively. The ultrahigh thermal rectification is found to be a result of the obvious phonon spectra mismatch before and after reversing the applied thermal bias. This outcome is attributed to both the device shape asymmetry and the size asymmetric boundary thermal contacts. We also find that the significant and stable standing waves that exist in graded two-stage pillared graphene structures play an important role in this kind of thermal rectifier, and are responsible for the ultrahigh thermal rectification of the two-stage ones as well. Our work demonstrates that pillared graphene structure with SWCNT−graphene intramolecular junctions is an excellent and promising phononic device.

KEYWORDS: *thermal rectification, pillared graphene, phonon density of states, standing wave, carbon nanotube-graphene intramolecular junctions, molecular dynamics*

Thermal rectifier is the most fundamental thermal/phononic device that controls the heat/phonon flow preferably in one direction. Because of its great potential in applications requiring thermal management,[1−5] there has been great interest in exploring new nanostructure with thermal rectification effect and studying novel thermal rectification mechanism.[6−15] For example, Chang et al.[1] have realized nanotube based thermal rectifier experimentally. As a primary building block for phononics, a thermal rectifier or diode is expected to act as a good thermal conductor if a positive thermal bias is applied and a poor thermal conductor in the opposite case of a negative thermal bias. Therefore, thermal rectifiers with high rectification ratio are highly desired, and finding more effective thermal rectifiers is highly important for future applications.

Three-dimensional (3D) pillared SWCNT−graphene nanostructures (PGNs) constructed with graphene layers as floors and SWCNTs as pillars hold great promise for future thermal interface materials.[16] Such nanostructure was first presented by Dimitrakakis et al. in 2008 for enhanced hydrogen storage,[17] and many experimental works in synthesis and processing have exhibited the feasibility of constructing PGNs in the laboratory.[18−20] Although there have been some studies[21−24] on the thermal conduction of SWCNT−graphene junction and 3D PGNs, whether thermal rectifier with high rectification efficiency can be constructed by using SWCNT−graphene junctions and 3D PGNs is unknown yet.

Recently, Lee et al.[7] and Liu et al.[25,26] found and proved that an important mechanism for thermal rectification in graded nanostructure is the existence of standing waves by simulations.

Received: October 10, 2016
Accepted: December 12, 2016
Published: December 12, 2016

DOI: 10.1021/acsami.6b12853
ACS Appl. Mater. Interfaces 2017, 9, 29−35

The standing wave is generated when the narrow end of the graded nanostructure is at a higher temperature than the wide end, and greatly hinders the propagation of phonon waves and the transfer of the thermal energy. The standing waves play an important role in thermal rectification in graded nanostructure, and its function is like the effect of phonon resonance, which has been reported in periodic array of pillars erected on the free surfaces.[26−28] The primary advantage of this structure is that the numerous local resonances of the pillars couple or hybridize with the underlying atomic-level phonon dispersion of the thin film across its spectrum. Thus, we will take advantage of these findings by designing a thermal rectifier using pillared graphene structure with SWCNT−graphene intramolecular junctions.

In this letter, using nonequilibrium molecular dynamics (NEMD) simulations along with the optimized Tersoff potential,[29] simulations are performed to investigate the thermal rectification of CNT−graphene junctions and 3D PGNs. We found that pillared graphene structures with SWCNT−graphene intramolecular junctions can exhibit ultrahigh thermal rectification; especially the designed pillared graphene structure in this work can reach 790.8 and 1173.0% at temperatures of 300 and 200 K, respectively.

First, NEMD simulations are conducted for PGNs using the LAMMPS software package.[30] To facilitate comparing with literature data, the simulation strategy adopted are almost same as that by Wang et al.,[8] including the method of thermostat, interatomic potential, simulation time steps, and so on. Schematics of the configuration for SWCNT-graphene intramolecular junctions are shown in Figure 1a, b. The atoms at the two ends are fixed, and free boundary conditions are applied to the other two directions. In all the schematic diagrams for calculation of thermal rectification, green, red and cyan area denote the fixed part, thermostated part and free part of the system. A relaxation for the PGNs are carried out under NVT ensemble at T_0 for 5×10^6 time steps (0.4 fs/time step) using the Nosé−Hoover thermostat, where T_0 is the average temperature of the system. Then NEMD is conducted for another 12×10^6 timesteps in the NVE ensemble to form a temperature gradient along the tube axial direction. Following the suggestion by Wang et al.,[8] Berendsen thermostat[23] are adopted for the heat and cold baths. We set temperature T_0 $(1+\Delta)$ for the bath of wide side and T_0 $(1-\Delta)$ the bath of narrow side. Δ is the normalized temperature difference between the baths of wide and narrow side. The heat flux due to the applied temperature bias can be calculated as $J = (\partial E_{hot}/\partial t + \partial E_{cold}/\partial t)/2$, where E_{hot} and E_{cold} are the total energy that has been exchanged from the atoms in the hot and cold thermostats, respectively.

The thermal rectification (TR) ratio is defined as

$$\eta = \frac{(J_+ - J_-)}{J_-} 100\% \quad (1)$$

where J_+ is the heat flow from wide side to narrow side which corresponds to $\Delta > 0$, and J_- is the heat flow from narrow side to wide side when $\Delta < 0$.

We first examine the thermal rectification of two different models of SWCNT-graphene intramolecular junctions, model TRA and model TRB, as shown in Figure 1. Following the idea of Lee, the free part of the system in Model TRA and Model TRB are considered as the nanodevice, and the thermostated parts can be considered as the thermal contacts. Thus, the model TRA is shape symmetric nanodevice with asymmetric in

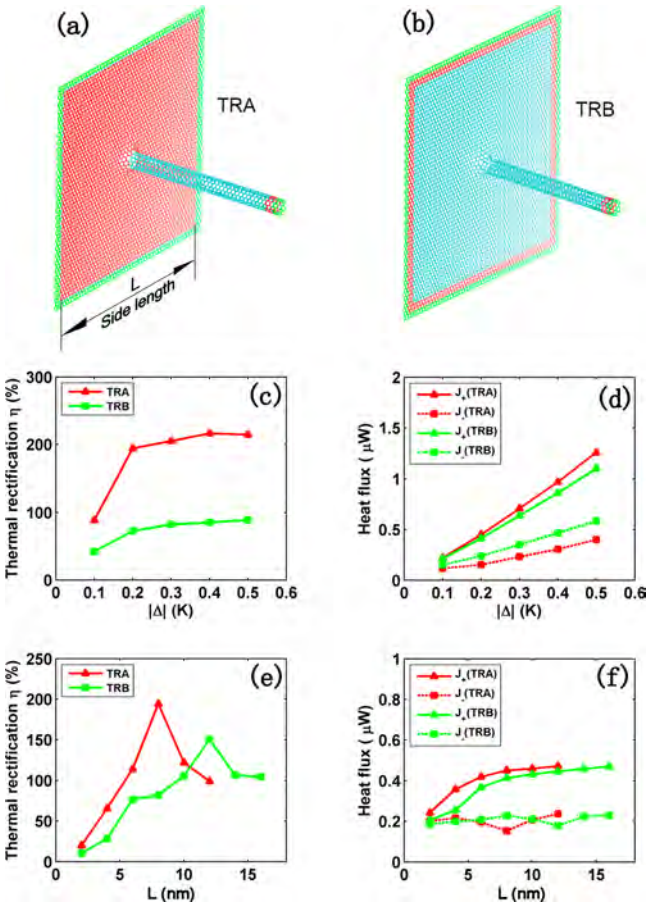

Figure 1. Calculation of thermal rectification and TR ratio and heat flux for Model TRA and TRB of SWCNT-graphene intramolecular junctions: (a) model TRA,(b) model TRB. Green, red and cyan areas denote the fixed part, thermostated part and free part of the system. (c) TR ratio vs |Δ| for TRA and TRB; (d) Heat flux vs |Δ|for TRA and TRB; (e) TR ratio vs side length of the graphene nanoribbon; (f) heat flux vs side length of the graphene nanoribbon. Δ is the normalized temperature difference between the baths of wide and narrow side, L is the side length of the graphene nanoribbon excluding the width of the fixed region.

boundary thermal contacts, whereas both the nanodevice and boundary thermal contacts in model TRB are asymmetric. The nanotube lengths for TRA and TRB are 9.5 nm. To facilitate the comparison of the size dependence of the graphene nanoribbon (GNR) on the thermal rectification effect, the side length of the GNR exclude the width of the fixed region.

Both TRA and TRB, the thermal rectification, are strongly size- and temperature-difference-dependent. The |Δ| dependence of thermal rectification ratio and heat flux for Model TRA and TRB are shown in Figure 1c, d, where the side length of the GNR region of TRA and TRB are designed as 8 nm. The behavior of the temperature difference dependence of thermal rectification and heat flux for TRA and TRB are very similar. The heat flux J versus temperature difference |Δ| is shown in Figure 1d. When $\Delta > 0$, J_+ increases steadily with Δ, whereas $\Delta < 0$, J_- is smaller. This indicates that the heat flux runs preferentially along the direction from the wide side to the narrow side in the junction model TRA and TRB. The corresponding thermal rectification ratio versus temperature difference is shown in Figure 1c. It can be observed that both TRA and TRB have good thermal rectification even when

DOI: 10.1021/acsami.6b12853
ACS Appl. Mater. Interfaces 2017, 9, 29−35

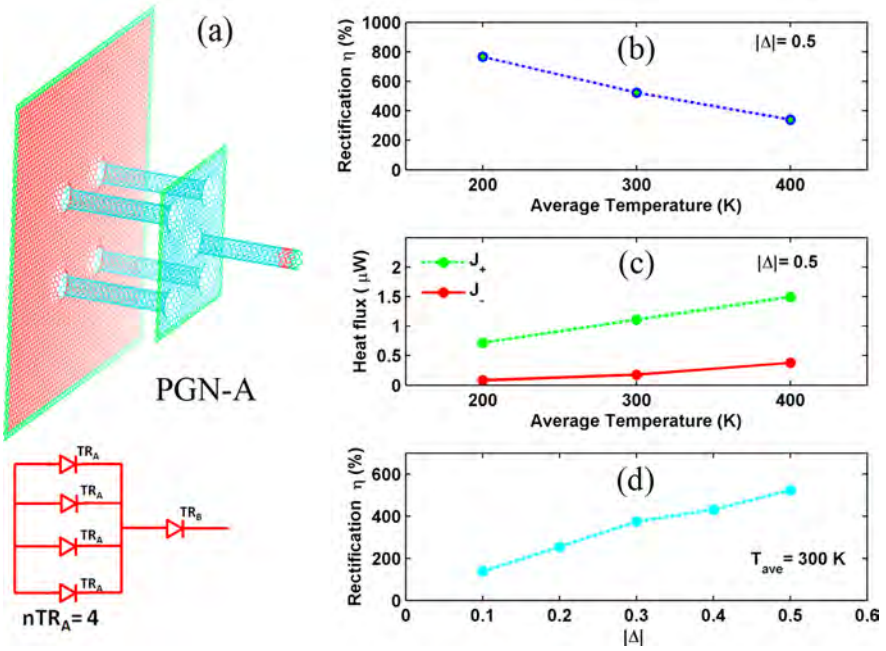

Figure 2. TR ratio and heat flux for pillared graphene structure PGN-A: (a) Schematic diagram of PGN-A for calculation of thermal rectification; green, red, and cyan areas denote the fixed part, thermostated part, and free part of the system. (b) TR ratio vs average temperature for PGN-A; (c) heat flux vs average temperature for PGN-A ; (d) TR ratio vs |Δ| for PGN-A.

temperature differences are small, |Δ| = 0.1; At room temperature and with |Δ|≥ 0.2, the rectification ratio of TRA can approach about 200%.

To understand the size dependence of the graphene region on the effect of the thermal rectification, we investigated thermal rectification of TRA and TRB with different-sized graphene regions. The heat flux vs side length of the GNR is shown in Figure 1f, whereas the TR ratio vs side length of the GNR is shown in Figure 1e. Here |Δ| is set as 0.2. The TR ratio first increases with the side length of the GNR region, reaches a peak value when side length GNR is 8 nm, and then begins to decrease with the side length of the GNR region. This implies that increasing the side length of GNR to enlarge the size asymmetric cannot always enhance the rectification ratio. For TRB, the curve also rises first and then falls, and the maximum value appears at the side length of the GNR region of 12 nm.

It can be observed from Figure 1f that the drop in the heat current J_- corresponds to the peak values of TR ratio in Figure 1e when the side length is 8 nm for TRA and 12 nm for TRB. It means both TR ratio and their corresponding heat flux are sensitive to the side length. In addition, the reason for the drop in the heat current J_- when the side length is 8 nm for TRA is explained in detail in the Supporting Information, and the explanation for the case of 12 nm for TRB is similar.

Lee et al.[7] have reported asymmetry in boundary thermal contacts play an important role in the thermal rectification in shape asymmetric nanodevice. Although they have demonstrated the size asymmetry in boundary thermal contacts can significantly affect the magnitude of thermal rectification, it is still unclear whether the thermal rectification in shape symmetric nanodevice with asymmetric boundary thermal contacts is a result of both the effects of shape asymmetry and the asymmetry in boundary thermal contacts. In the system of the investigation of Lee et al., the device and the thermal contact are seamlessly contacted, and both the thermal contact reservoirs and the nanodevice in their system are in the same crystalline material. Following their strategy, in TRA as shown in Figure 1a, a shape symmetric nanostructure, carbon nanotube, can be considered as the device in the system, and the thermostated part of the GNR region and SWCNT region on the two sides can serve as the thermal contact reservoirs. Thus, it implies that the asymmetry in boundary thermal contacts can solely determine the thermal rectification in a shape symmetric nanodevice. The effect of the size asymmetric boundary thermal contacts on thermal rectification is even more significant than that of the device shape asymmetry.

As obtained from above, SWCNT−graphene intramolecular junctions have exhibited good potential as thermal rectifier; however, their thermal rectifications are still limited. Therefore, in the following, we will investigate how to design a more efficient multilevel thermal rectifier using the SWCNT−graphene intramolecular junctions as building blocks.

We first construct a graded two-stage thermal rectifier, PGN-A, using the above TRA and TRB as building blocks, as shown in Figure 2a. It can be considered as consisting of 4 TRA and one TRB. The tube length in TRA part is about 4.8 nm and the tube length in TRB part is about 4.67 nm. The side length of the GNR on the left (excluding its fixed part) is 14 nm, and the side length of the GNR in the middle (excluded its fixed part) is 6 nm, where the width of the fixed region is set as 0.4 nm. Here the size of each component in PGN-A and PGN-B is not optimized. When setting the size for PGN-A and PGN-B, we just want to make the external profile of the nanostructures look more like a cone as a whole in order to make a graded pillared graphene structures.

For PGN-A, the thermal rectification ratio and the heat flux J versus average temperature are shown in Figure 2b, c respectively. Interestingly, such a pillared graphene structures with SWCNT-graphene intramolecular junctions can exhibit very high thermal rectification. Specially, the designed pillared graphene structure in this work can reach 523 and 766% at temperature 300 and 200 K, respectively.

DOI: 10.1021/acsami.6b12853
ACS Appl. Mater. Interfaces 2017, 9, 29−35

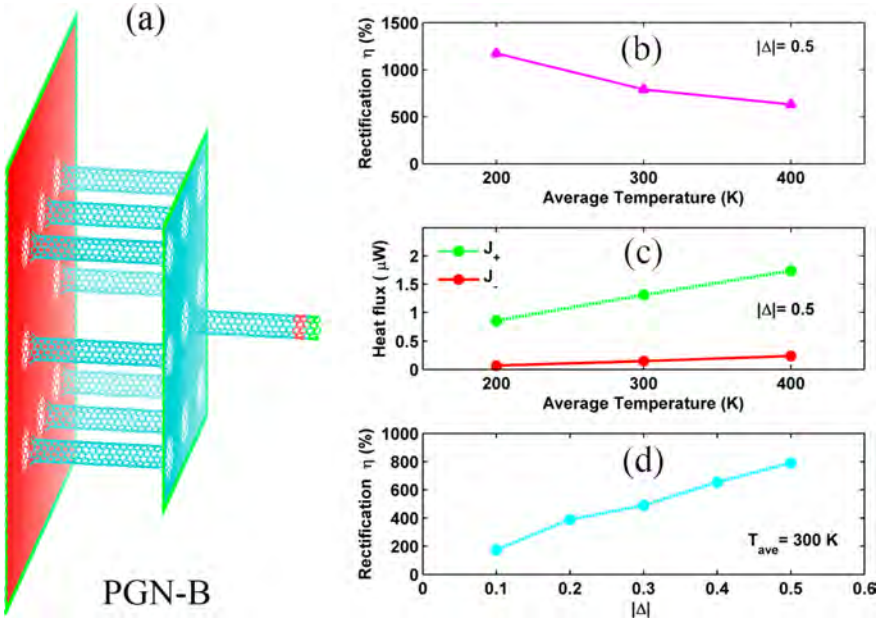

Figure 3. TR ratio and heat flux for pillared graphene structure PGN-B: (a) Schematic diagram of PGN-B for calculation of thermal rectification; green, red, and cyan areas denote the fixed part, thermostated part, and free part of the system. (b) TR ratio vs average temperature for PGN-B; (c) heat flux vs average temperature for PGN-B; (d) TR ratio vs |Δ| for PGN-B.

Moreover, we also construct a graded two-stage thermal rectifier, PGN-B, consisting of 8 TRA and one TRB, as shown in Figure 3a. The tubes length are same as those in PGN-A. The side length of the GNR on the left (excluded its fixed part) is 16 nm, and the side length of the GNR in the middle (excluding its fixed part) is 10 nm, where the width of the fixed region is set as 0.4 nm. For PGN-B, the thermal rectification ratio and the heat flux J versus average temperature are shown in Figure 3b, c, respectively. Surprisingly, such a pillared graphene structures with SWCNT-graphene intramolecular junctions can exhibit ultrahigh thermal rectification reaching 790.8 and 1173.0% at temperature 300 and 200 K, respectively.

We definitely believe thermal rectifier with much higher thermal rectification than PGN-B can be constructed by using more TRAs in the second stage and more stages and optimizing the size of each components. All this work will be farther investigated in our future work, which may require more computational cost. Anyways, we have proposed and demonstrated a novel method to build a thermal rectifier with ultrahigh thermal rectification ratio.

To understand the underlying mechanism of the ultrahigh thermal rectification in graded pillared graphene structure, we calculate the power spectra of both the pillared graphene structure and SWCNT-graphene intramolecular junctions. The power spectrum has been considered as a good qualitative and quantitative method to explain the heat rectification effect. Similar to that in ref 7, in our calculation, only the free parts in the system are considered to be the device, and the thermostated parts are considered to be the thermal contacts. In the vibration density of states (vDOS) calculation, we choose the atoms of the device in the first two unit cells away from each thermal contact

As shown in Figure 4a, c for TRA and TRB, $\Delta > 0$, the power spectra of the wide and narrow sides of the device overlap relatively well in the frequency range. It means the phonons can go through the device easily with a large J_+. Conversely, when $\Delta < 0$ in Figure 4b, d, obvious mismatch in the power spectra can be observed in both low and high frequency region. The large mismatch means the weak correlation between the two ends of the device, therefore the phonons are difficult to go through the device and thus lead to very small J_-.

Similarly as shown in Figure 4e–h for PGN-A and PGN-B, the power spectra of the wide and narrow sides overlap well under positive thermal bias, and more obvious phonon spectrum mismatch with very significant low frequency peaks appear under negative thermal bias. The vDOS of the narrow side is much more sensitive to the temperature change and high temperature than that of the wide side, resulting in a pronounced mismatch in vDOS when $\Delta < 0$. In fact, such an emergence of low-frequency modes in the vDOS of the narrow side under negative thermal bias has been well-explained in details in ref 7. The strategy adopted in our simulations is almost the same as that in ref 7, except we use Berendsen thermostat rather than the Nosé–Hoover thermostat for the hot and cold bath. More importantly, in the Supporting Information, it is clear that the calculated results of the ultrahigh thermal rectification for PGN-B by using Berendsen thermostat and the Nosé–Hoover thermostat for the thermal reservoir is almost same, and very significant low frequency peaks appear under negative thermal bias in both these two cases. Thus, the ultrahigh thermal rectification for PGN-A and PGN-B could be well-understood.

The match or mismatch of the vDOS between the wide and narrow sides of the device leads to the rectification phenomenon. To quantify the analysis of the match or mismatch of the vDOS, the overlaps (S) of the vDOS of the wide and narrow sides of the device are calculated as follows

$$S_{\pm} = 1 - \frac{\int |P_w(\omega) - P_n(\omega)| d\omega}{\left(\int P_w(\omega) d\omega \int P_n(\omega) d\omega\right)^{1/2}} \quad (2)$$

Here $S_{\pm}$ corresponds to the case of $\Delta > 0$ and $\Delta < 0$, respectively, $P_w(\omega)$ is the power spectrum of the wide sides of the device, and $P_n(\omega)$ is the power spectrum of the narrow

DOI: 10.1021/acsami.6b12853
ACS Appl. Mater. Interfaces 2017, 9, 29–35

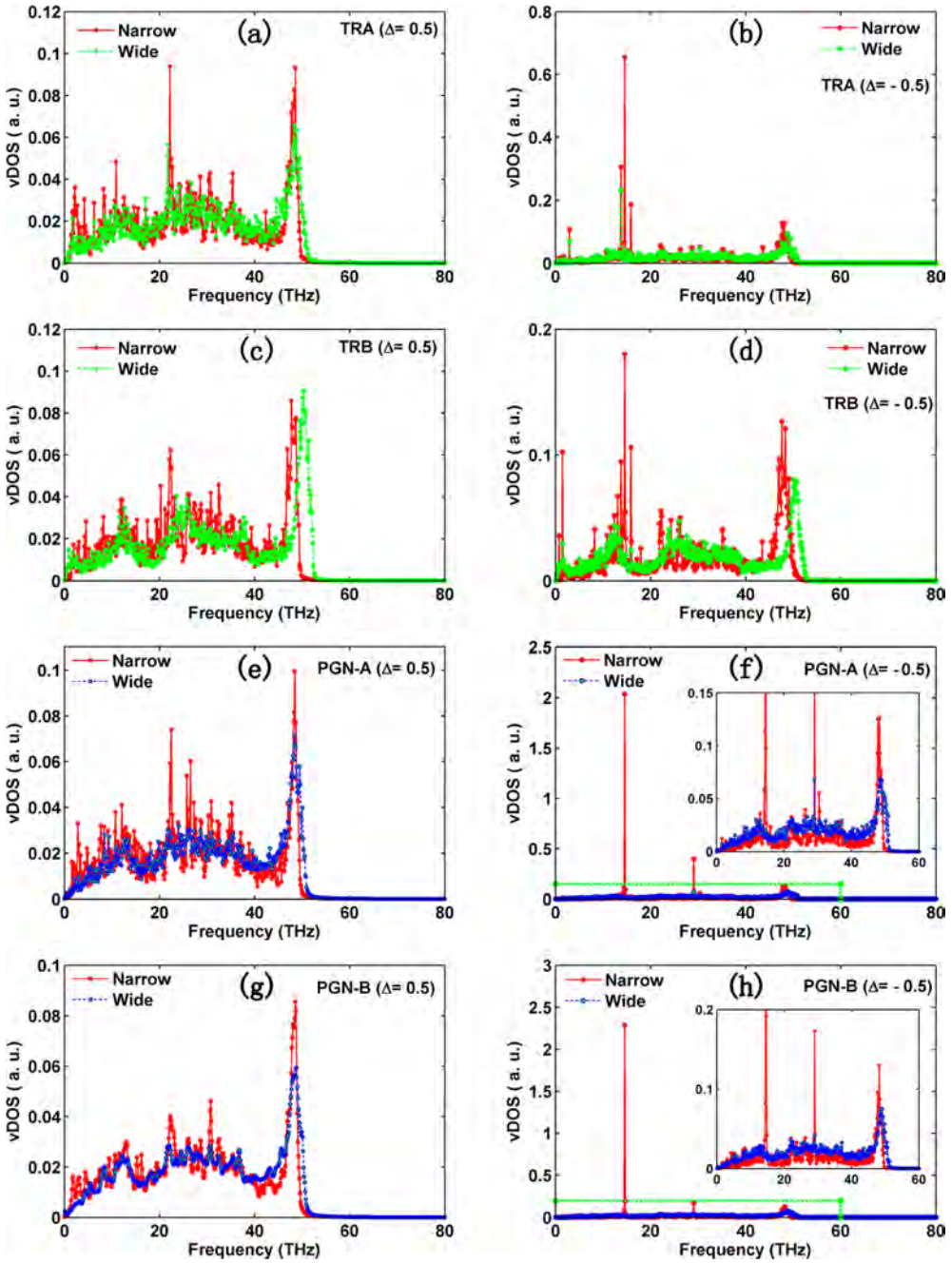

Figure 4. Vibrational density of states (vDOS) per atom: (a) TRA,Δ = 0.5; (b)TRA, Δ = −0.5; (c) TRB,Δ = 0.5; (d)TRB, Δ = −0.5; (e) PGN-A, Δ = 0.5; (f) PGN-A, Δ = −0.5; (g) PGN-B, Δ = 0.5; (h) PGN-B, Δ = −0.5.

sides of the device. In Figure 4, the calculated S_+/S_- ratios for TRA, TRB, PGN-A, and PGN-B are 1.48, 1.21, 2.90, and 3.02, respectively. The calculated S_+/S_- ratios for two-stage thermal rectifiers PGN-A and PGN-B are much larger than the single-stage thermal rectifiers TRA and TRB, which should be the reason why the rectification ratios of PGN-A and PGN-B are much higher than TRA and TRB.

We also tried to explain why the two-stage thermal rectifier PGN-A and PGN-B have much larger thermal rectification ratio comparing with the one-stage thermal rectifier TRA and TRB from the aspect of the standing wave, because some sharp peaks in vDOS for the narrow ends suggest that the corresponding vibration modes seem to be of standing wave nature. To confirm the existence of the standing wave, we calculated the velocity autocorrelation function (VACF) of the groups of atoms at the narrow ends for TRA, TRB, PGN-A, and PGN-B and shown in Figure 5, which correspond to the atoms group whose vDOS have been calculated and shown above. In Figure 5a, c for TRA and TRB, the periodicity of the VACF indicates their original signal, the velocities have periodic component (although is not so stable for TRB), standing waves have been generated but are not strong enough to dominate the vibration. For the VACF of the PGN-A and PGN-B shown in Figure 5e, g, the formation of the standing wave is obvious and has dominated the vibration at the narrow end. Thus, it indicates that the two-stage thermal rectifier PGN-A and PGN-B are more apt to form significant standing wave than the single-stage thermal rectifier TRA and TRB. It can be observed from

DOI: 10.1021/acsami.6b12853
ACS Appl. Mater. Interfaces 2017, 9, 29−35

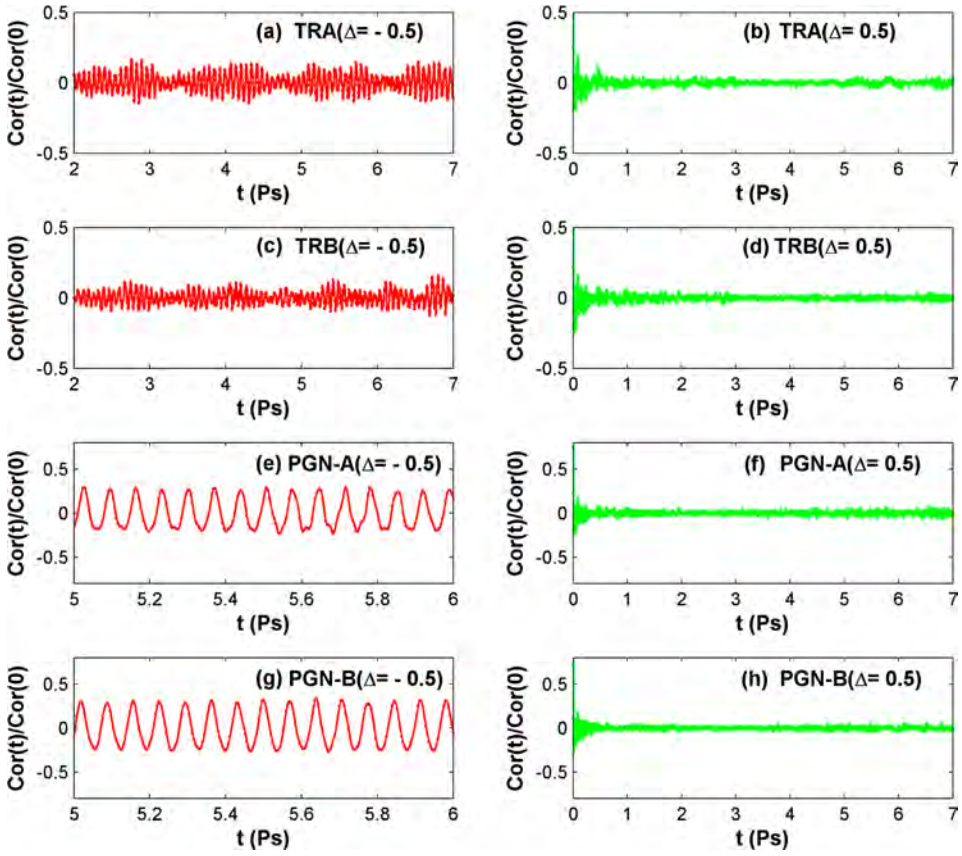

Figure 5. Normalized velocity autocorrelation functions for (a) TRA,Δ = −0.5; (b)TRA, Δ = 0.5; (c) TRB,Δ = −0.5; (d)TRB, Δ = 0.5; (e) PGN-A, Δ = −0.5; (f) PGN-A, Δ = 0.5; (g) PGN-B, Δ = −0.5; (h) PGN-B, Δ = 0.5.

Figures 2c and 3c that the heat flux in PGN-B is much less than that in PGN-A, which indicates that the stronger the standing wave, the less heat will be transported in the system, and the thermal conductivity of which will be more significantly reduced. We also conclude that the significant increase in the thermal rectification ratio of PGN-A and PGN-B is due to the generation of more significant standing waves.

The calculated frequency of the standing wave in PGN-A and PGN-B shown in Figure 5e, g is 14.5 THz, which corresponds to the frequency of the sharp peaks (14.5 THz and 29 THz) in the vDOS analysis. Additionally, when Δ < 0, in PGN-A and PGN-B, with more parallel thermal rectifier TRA connected at the second stage, some of the phonon modes can be significantly suppressed in the thermal transport; especially, the value of the peak at ∼29 THz in PGN-B at the wide end is almost half of that in PGN-A, which means the thermal flux across the system is further limited. In addition, it can be seen from the Figure 5b, d, f, and h that the VACFs of the atoms near the narrow end decayed to zero around 1 ps with negligible fluctuation. This means no standing waveform at the narrow side when Δ > 0.

We have demonstrated that SWCNT-graphene intramolecular junctions are promising thermal rectifiers themselves, and more importantly, they can be used as building blocks for constructing more efficient thermal rectifiers with ultrahigh thermal rectification ratio.

In summary, we demonstrate that pillared graphene structures with SWCNT-graphene intramolecular junctions can exhibit ultrahigh thermal rectification. Specifically, the designed pillared graphene structure in this work can reach 790.8% and 1173.0% at temperatures 300 and 200 K, respectively. The ultrahigh thermal rectification is attributed to both the device shape asymmetry and the size asymmetric boundary thermal contacts, and the effect of the size asymmetric boundary thermal contacts is even more significant than that of the device shape asymmetry. Our work demonstrates that pillared graphene structure with SWCNT−graphene intramolecular junctions is an excellent and promising practical phononic device.

■ ASSOCIATED CONTENT

Ⓢ Supporting Information

The Supporting Information is available free of charge on the ACS Publications website at DOI: 10.1021/acsami.6b12853.

Comparison of the calculated results of the thermal rectification for PGN-B by using Berendsen thermostat and the Nosé−Hoover thermostat for the thermal reservoir, vDOS per atom for PGN-B using the Nosé−Hoover thermostat, normalized velocity autocorrelation functions when Δ= −0.5 for PGN-B using the Nosé−Hoover thermostat; calculated natural frequencies of PGN-A and PGN-B; an explanation for the drop in the heat current J_- when the side length is 8 nm for TRA and 12 nm for TRB (PDF)

■ AUTHOR INFORMATION

Corresponding Authors

*E-mail: ncepub@hotmail.com.
*E-mail: caoby@tsinghua.edu.cn.

DOI: 10.1021/acsami.6b12853
ACS Appl. Mater. Interfaces 2017, 9, 29−35

ORCID

Xueming Yang: 0000-0001-7309-7817

Notes

The authors declare no competing financial interest.

■ ACKNOWLEDGMENTS

This research is supported by the National Natural Science Foundation of China (Grants 51576066, 51322603, 51136001, and 51356001), the Natural Science Foundation of Hebei Province of China (Grant E2014502042), and the China Postdoctoral Science Foundation (Grant 2015M570095).

■ REFERENCES

(1) Chang, C. W.; Okawa, D.; Majumdar, A.; Zettl, A. Solid-State Thermal Rectifier. *Science* **2006**, *314*, 1121−1124.
(2) Li, N.; Ren, J.; Wang, L.; Zhang, G.; Hänggi, P.; Li, B. Colloquium: Phononics: Manipulating Heat Flow With Electronic Analogs and Beyond. *Rev. Mod. Phys.* **2012**, *84*, 1045.
(3) Li, B.; Wang, L.; Casati, G. Thermal Diode: Rectification of Heat Flux. *Phys. Rev. Lett.* **2004**, *93*, 184301.
(4) Wang, L.; Li, B. Thermal Logic Gates: Computation with Phonons. *Phys. Rev. Lett.* **2007**, *99*, 177208.
(5) Wang, L.; Li, B. Thermal Memory: a Storage of Phononic Information. *Phys. Rev. Lett.* **2008**, *101*, 267203.
(6) Hu, J.; Ruan, X.; Chen, Y. P. Thermal Conductivity and Thermal Rectification in Graphene Nanoribbons: a Molecular Dynamics Study. *Nano Lett.* **2009**, *9*, 2730−2735.
(7) Lee, J.; Varshney, V.; Roy, A. K.; Ferguson, J. B.; Farmer, B. L. Thermal Rectification in Three-Dimensional Asymmetric Nanostructure. *Nano Lett.* **2012**, *12*, 3491−3496.
(8) Wang, Y.; Vallabhaneni, A.; Hu, J.; Qiu, B.; Chen, Y. P.; Ruan, X. Phonon Lateral Confinement Enables Thermal Rectification in Asymmetric Single-Material Nanostructures. *Nano Lett.* **2014**, *14*, 592−596.
(9) Zhang, G.; Zhang, H. Thermal Conduction and Rectification in Few-Layer Graphene Y Junctions. *Nanoscale* **2011**, *3*, 4604−4607.
(10) Zhang, T.; Luo, T. Giant Thermal Rectification from Polyethylene Nanofiber Thermal Diodes. *Small* **2015**, *11*, 4657−4665.
(11) Yang, N.; Zhang, G.; Li, B. Carbon Nanocone: a Promising Thermal Rectifier. *Appl. Phys. Lett.* **2008**, *93*, 243111.
(12) Cartoixà, X.; Colombo, L.; Rurali, R. Thermal Rectification by Design in Telescopic Si Nanowires. *Nano Lett.* **2015**, *15*, 8255−8259.
(13) Bui, K.; Nguyen, H.; Cousin, C.; Striolo, A.; Papavassiliou, D. V. Thermal Behavior of Double-Walled Carbon Nanotubes and Evidence of Thermal Rectification. *J. Phys. Chem. C* **2012**, *116*, 4449−4454.
(14) Zhang, L.; Wang, J. S.; Li, B. Ballistic Thermal Rectification in Nanoscale Three-Terminal Junctions. *Phys. Rev. B: Condens. Matter Mater. Phys.* **2010**, *81*, 100301.
(15) Gunawardana, K. G. S. H.; Mullen, K.; Hu, J.; Chen, Y. P.; Ruan, X. Tunable Thermal Transport and Thermal Rectification in Strained Graphene Nanoribbons. *Phys. Rev. B: Condens. Matter Mater. Phys.* **2012**, *85*, 245417.
(16) Park, J.; Prakash, V. Thermal Transport in 3D Pillared SWCNT−Graphene Nanostructures. *J. Mater. Res.* **2013**, *28*, 940−951.
(17) Dimitrakakis, G. K.; Tylianakis, E.; Froudakis, G. E. Pillared Graphene: a New 3-D Network Nanostructure for Enhanced Hydrogen Storage. *Nano Lett.* **2008**, *8*, 3166−3170.
(18) Fan, Z.; Yan, J.; Zhi, L.; Zhang, Q.; Wei, T.; Feng, J.; Zhang, M.; Qian, W.; Wei, F. A Three-Dimensional Carbon Nanotube/Graphene Sandwich and Its Application as Electrode in Supercapacitors. *Adv. Mater.* **2010**, *22*, 3723−3728.
(19) Du, F.; Yu, D.; Dai, L.; Ganguli, S.; Varshney, V.; Roy, A. K. Preparation of Tunable 3D Pillared Carbon Nanotube−Graphene Networks for High-Performance Capacitance. *Chem. Mater.* **2011**, *23*, 4810−4816.
(20) Paul, R. K.; Ghazinejad, M.; Penchev, M.; Lin, J.; Ozkan, M.; Ozkan, C. S. Synthesis of a Pillared Graphene Nanostructure: A Counterpart of Three-Dimensional Carbon Architectures. *Small* **2010**, *6*, 2309−2313.
(21) Varshney, V.; Patnaik, S. S.; Roy, A. K.; Froudakis, G.; Farmer, B. L. Modeling of Thermal Transport In Pillared-Graphene Architectures. *ACS Nano* **2010**, *4*, 1153−1161.
(22) Xu, L.; Wei, N.; Zheng, Y.; Fan, Z.; Wang, H. Q.; Zheng, J. C. Graphene-Nanotube 3D Networks: Intriguing Thermal and Mechanical Properties. *J. Mater. Chem.* **2012**, *22*, 1435−1444.
(23) Bao, H.; Shao, C.; Luo, S.; Hu, M. Enhancement of Interfacial Thermal Transport by Carbon Nanotube-Graphene Junction. *J. Appl. Phys.* **2014**, *115*, 053524.
(24) Shi, J.; Dong, Y.; Fisher, T.; Ruan, X. Thermal Transport Across Carbon Nanotube-Graphene Covalent and Van Der Waals Junctions. *J. Appl. Phys.* **2015**, *118*, 044302.
(25) Liu, Y. Y.; Zhou, W. X.; Chen, K. Q. Conjunction of Standing Wave and Resonance in Asymmetric Nanowires: a Mechanism for Thermal Rectification and Remote Energy Accumulation. *Sci. Rep.* **2015**, *5*, 17525.
(26) Liu, Y. Y.; Zhou, W. X.; Tang, L. M.; Chen, K. Q. An Important Mechanism for Thermal Rectification in Graded Nanowires. *Appl. Phys. Lett.* **2014**, *105*, 203111.
(27) Davis, B. L.; Hussein, M. I. Nanophononic Metamaterial: Thermal Conductivity Reduction by Local Resonance. *Phys. Rev. Lett.* **2014**, *112*, 055505.
(28) Pennec, Y.; Djafari-Rouhani, B.; Larabi, H.; Vasseur, J. O.; Hladky-Hennion, A. C. Low-Frequency Gaps in a PhononicCrystal Constituted of Cylindrical Dots Deposited on a Thin Homogeneous Plate. *Phys. Rev. B: Condens. Matter Mater. Phys.* **2008**, *78*, 104105.
(29) Lindsay, L.; Broido, D. A. Optimized Tersoff and Brenner Empirical Potential Parameters for Lattice Dynamics and Phonon Thermal Transport in Carbon Nanotubes and Graphene. *Phys. Rev. B: Condens. Matter Mater. Phys.* **2010**, *81*, 205441.
(30) Plimpton, S. Fast Parallel Algorithms forShort-Range Molecular Dynamics. *J. Comput. Phys.* **1995**, *117*, 1−19.

DOI: 10.1021/acsami.6b12853
ACS Appl. Mater. Interfaces 2017, 9, 29−35